salto/CG13164 is required for sperm head morphogenesis in *Drosophila*

Céline Augière, Jean-André Lapart, Jean-Luc Duteyrat, Elisabeth Cortier, Charline Maire, Joëlle Thomas, and Bénédicte Durand*
Université de Lyon, Université Claude Bernard Lyon 1, CNRS UMR-5310, INSERM U-1217, Institut NeuroMyoGène, F-69008 Lyon, France

ABSTRACT **Producing mature spermatozoa is essential for sexual reproduction in metazoans. Spermiogenesis involves dramatic cell morphological changes going from sperm tail elongation and nuclear reshaping to cell membrane remodeling during sperm individualization and release. The sperm manchette plays a critical scaffolding function during nuclear remodeling by linking the nuclear lamina to the cytoskeleton. Here, we describe the role of an uncharacterized protein in *Drosophila*, *salto/CG13164*, involved in nuclear shaping and spermatid individualization. Salto has dynamic localization during spermatid differentiation, being progressively relocated from the sperm-nuclear dense body, which is equivalent to the mammalian sperm manchette, to the centriolar adjunct and acrosomal cap during spermiogenesis. *salto*-null male flies are sterile and exhibit complete spermatid individualization defects. *salto*-deficient spermatids show coiled spermatid nuclei at late maturation stages and stalled individualization complexes. Our work sheds light on a novel component involved in cytoskeleton-based cell-morphological changes during spermiogenesis.**

Monitoring Editor
Julie Brill
The Hospital for Sick Children

Received: Jul 12, 2018
Revised: Dec 20, 2018
Accepted: Dec 27, 2018

INTRODUCTION

Both in mammals and in insects, spermiogenesis involves severe cell morphological changes, including sperm tail elongation, nuclear remodeling, and ultimately sperm individualization, also called spermiation (Fabian and Brill, 2012; O'Donnell, 2014). Nuclear elongation is associated with DNA condensation and involves different sets of proteins (Rathke *et al.*, 2007). Whereas protamines and transition proteins are involved in chromatin condensation, nuclear elongation requires proteins of both the inner and outer nuclear membranes and involves perinuclear microtubules (Fabian and Brill, 2012; O'Donnell, 2014). In mammals and in *Drosophila*, proteins of the LINC complex link the nuclear envelope and nuclear lamina to the microtubule cytoskeleton (Kracklauer *et al.*, 2010; Lehti and Sironen, 2016). Specifically, SUN domain–containing proteins of the inner nuclear membrane are required for nuclear morphogenesis (Keller *et al.*, 2009; Kracklauer *et al.*, 2010; Calvi *et al.*, 2015). These SUN domain proteins interact with KASH domain–containing proteins of the outer nuclear membrane that link cytoplasmic microtubules (for reviews see Kierszenbaum, 2002; Lehti and Sironen, 2016). These perinuclear cytoplasmic microtubules are important for nuclear shaping during spermiogenesis. In *Drosophila*, the perinuclear microtubules compose the dense complex (DC), which is analogous to the mammalian manchette involved in sperm-head shaping (for review see Fabian and Brill, 2012). During spermatid differentiation, microtubules of the DC concentrate on the fenestrated side of the nuclei. Proteins such as Spag4 (SUN domain protein) and Yuri have been shown to distribute respectively on the inner nuclear membrane and along the microtubules of the DC and to interact functionally during nuclear elongation (Texada *et al.*, 2008; Kracklauer *et al.*, 2010; Sitaram *et al.*, 2012). During this process, Spag4 and Yuri progressively concentrate around the centriolar adjunct, a structure that is formed in the vicinity of the basal body, while it anchors to the nucleus during spermiogenesis. Hence, mutations in Spag4 or Yuri induce sperm nuclear–shaping defects together with disturbed basal body anchoring into the nucleus. The latter defect is independent of the integrity of the KASH domains of the only two KASH domain–containing proteins of *Drosophila*, Klarsicht and Msp300 (Kracklauer *et al.*, 2010). This suggests that still undiscovered specific components are needed to link SUN domain proteins of the nuclear membrane to the microtubule network and centriolar proteins.

This article was published online ahead of print in MBoC in Press (http://www.molbiolcell.org/cgi/doi/10.1091/mbc.E18-07-0429) on January 2, 2019.

*Address correspondence to: Bénédicte Durand (durand-b@univ-lyon1.fr).

Abbreviations used: Cby, Chibby; DC, dense complex; EM, electron microscopy; IC, individualization complex, investment cone.

Another important feature of spermiogenesis is the individualization of spermatids, also called spermiation, leading to the elimination of bulk cytoplasmic content and to sperm release (O'Donnell, 2014; Steinhauer, 2015). Individualization takes place once sperm head and tail have elongated completely. In *Drosophila*, this requires three successive steps: 1) recruitment of a specialized actin-based complex, the individualization complex (IC), 2) migration of this IC associated with membrane remodeling, and 3) elimination of excess material. These two last steps require the activation of a non-apoptotic caspase pathway (Fabian and Brill, 2012). IC migration along the 64 interconnected spermatids relies on the recruitment of specific molecular motors and removes most of the cytoplasm and organelles into a membrane-bound sack, called the cystic bulge, which is discarded as a waste bag when ICs reach the tip of the spermatids (Fabrizio *et al.*, 1998). Disturbing IC assembly or migration is correlated with defective individualization (Noguchi, 2003; Steinhauer, 2015). However, individualization failure can also be the ultimate consequence of various previous defects, including meiosis and flagellar assembly defects (Steinhauer, 2015).

In a two-hybrid screen (J.T. and J.A.L., unpublished data), using the ciliary transition zone protein Chibby (Cby; Enjolras *et al.*, 2012; Vieillard *et al.*, 2016) as bait, we have identified an uncharacterized protein encoded by *CG13164*, which is highly expressed in the testis (modENCODE, tissue expression data; Brown *et al.*, 2014). This protein was previously described as interacting with syntaxin and named Sip2 (for syntaxin–interacting protein2). Because of a potential confusion between *CG13164/sip2* and another gene, *SIP2 (septin interacting protein 2/CG9188*), and based on the mutant phenotype described hereafter, we renamed this gene *salto* (French for "somersault"). Although we could not confirm the interaction with Cby, we observed a critical function of this protein in spermiogenesis. We show that Salto is located at several major structures involved in sperm-head architecture and in particular with the sperm manchette/DC and centriolar adjunct. *salto*-null flies are sterile and show spermiogenesis defects characterized by abnormal nuclear coiling of late spermatids, leading to failure of sperm individualization. Actin cones can form but fail to migrate and elevated caspase activity is observed along the length of the spermatids. Because Salto distribution and mutant phenotype are similar to those observed for Spag4 and Yuri, our work suggests that all three proteins work in a common pathway required for sperm-head morphogenesis. *salto* hence represents a novel actor involved in spermiogenesis and sperm-head morphogenesis in *Drosophila*.

RESULTS

salto encodes a testis-specific protein in *Drosophila* that shows a dynamic distribution during spermatogenesis

We identified Salto in a yeast two-hybrid screen using full-length Chibby protein as bait (see *Materials and Methods*). All isoforms encoded by *salto* possess potential coiled-coil domains. Structural analysis indicates that Salto contains a pentapeptide repeat domain (12 repeats of the sequence LQEPN and five of LQD(A/D)(T/N)), found in the uncharacterized YjbI protein from *Escherichia coli*, and a putative SMC_N domain (Supplemental Figure S1B), found at the N-terminus of SMC proteins involved in chromatin maintenance (Strunnikov and Jessberger, 1999). From the CDART database (Geer *et al.*, 2002), only a few proteins share this domain architecture in the eukaryotic kingdom. Salto is conserved almost exclusively among arthropods and is found in all drosophilids. Outside arthropods, a possible homologue, containing the SMC_N domain but not the pentapeptide repeat domain, could be found only in *Ciona* (Supplemental Figure S1A). The SMC_N domain is the most conserved part of the protein. The NCBI conserved domain database (Marchler-Bauer *et al.*, 2017) also identifies a putative highly divergent BAR domain, but this homology is weak. Multiple pairwise analysis in comparison with other BAR-domain proteins in *Drosophila* indicate most similarities with the F-BAR domain containing the protein syndapin (38% similarities, and 19% identities with *Drosophila* syndapin; accession NP_732563.1).

In *Drosophila melanogaster*, *salto* potentially encodes four different transcripts (Figure 1A). We designed a reporter construct expressing the longest *salto* coding frame fused to GFP and under the control of its own promotor (Figure 1A) to create *salto::GFP*–expressing transgenic flies. We observed a very weak Salto–GFP signal at the tip of the sensory dendrites in chordotonal organs of embryos, suggesting that *salto* is expressed at a low level in sensory ciliated neurons (Supplemental Figure S2). Strikingly, *salto::GFP* expression is strong in the testis. Salto–GFP was detectable in all steps of spermatogenesis, from spermatocytes to fully elongated spermatids (Figure 1, B–H). In spermatocytes, Salto–GFP encages spermatocyte nuclei (Figure 1C, arrowhead). In addition, Salto–GFP forms a halo around centrioles and is located at the primary like cilium above the centrioles (Figure 1C, inset and arrows). Transition zone proteins like Cby also locate at this primary like cilium at this stage (Enjolras *et al.*, 2012; Pratt *et al.*, 2016; Vieillard *et al.*, 2016). At the onset of meiosis, high levels of Salto–GFP are observed at the forming spindle poles and decorate the microtubules (Figure 1D). After meiosis, Salto–GFP decorates a half dome encircling the nuclei and anchored to the basal body (Figure 1E). Such staining was previously described for Yuri and Spag4 as the nuclear "cap" (Kracklauer *et al.*, 2010) and likely corresponds at the round spermatid stage to the fenestrated part of the nucleus surrounded by the microtubule network of the sperm manchette or DC. After the beginning of flagellar elongation, Salto–GFP is relocated both to the centriolar adjunct (labeled with γ-tubulin antibodies; Wilson *et al.*, 1997) and to the acrosome (Figure 1F). When spermatids are fully elongated and before the beginning of individualization, Salto–GFP is mainly observed at the acrosome (Figure 1G). In mature sperm, after individualization, this protein is not detected (unpublished data). We also determined the localization of Salto–GFP after treating testes by colcemid. We observed that Salto–GFP signal at the spindle poles in spermatocytes or at the nuclear cap in early spermatids is strongly reduced when microtubule depolymerization is induced, whereas a distinct Salto–GFP signal along the axoneme is not affected by colcemid. Note that Salto–GFP is enriched at the distal growing tip of the axoneme in this colcemid-treated condition (Supplemental Figure S2, arrowheads). Altogether, these observations indicate that Salto–GFP is dynamically associated with the pericentriolar microtubules during meiosis and with the nuclear-associated manchette microtubule network required for nuclear shaping during spermiogenesis.

sal^{1}-null mutant males are sterile and show sperm individualization defects

To understand the function of Salto, we generated *salto*-null mutant flies (*sal*^{1} allele) by CRISPR-Cas9–mediated homologous recombination, replacing all *salto* coding sequences with the mini-white gene (Figure 2A). We confirmed by sequencing that the entire coding sequence of *salto* was replaced with the *white* gene. *sal*^{1} homozygous mutant flies and *sal*^{1} heterozygotes over a deletion that uncovers the *salto* locus (Df(2R)BSC463) are viable and show no obvious behavioral defects. Females are fertile (unpublished data), but males are sterile and do not produce mature sperm (Figure 2B). Male fertility could be partially rescued by

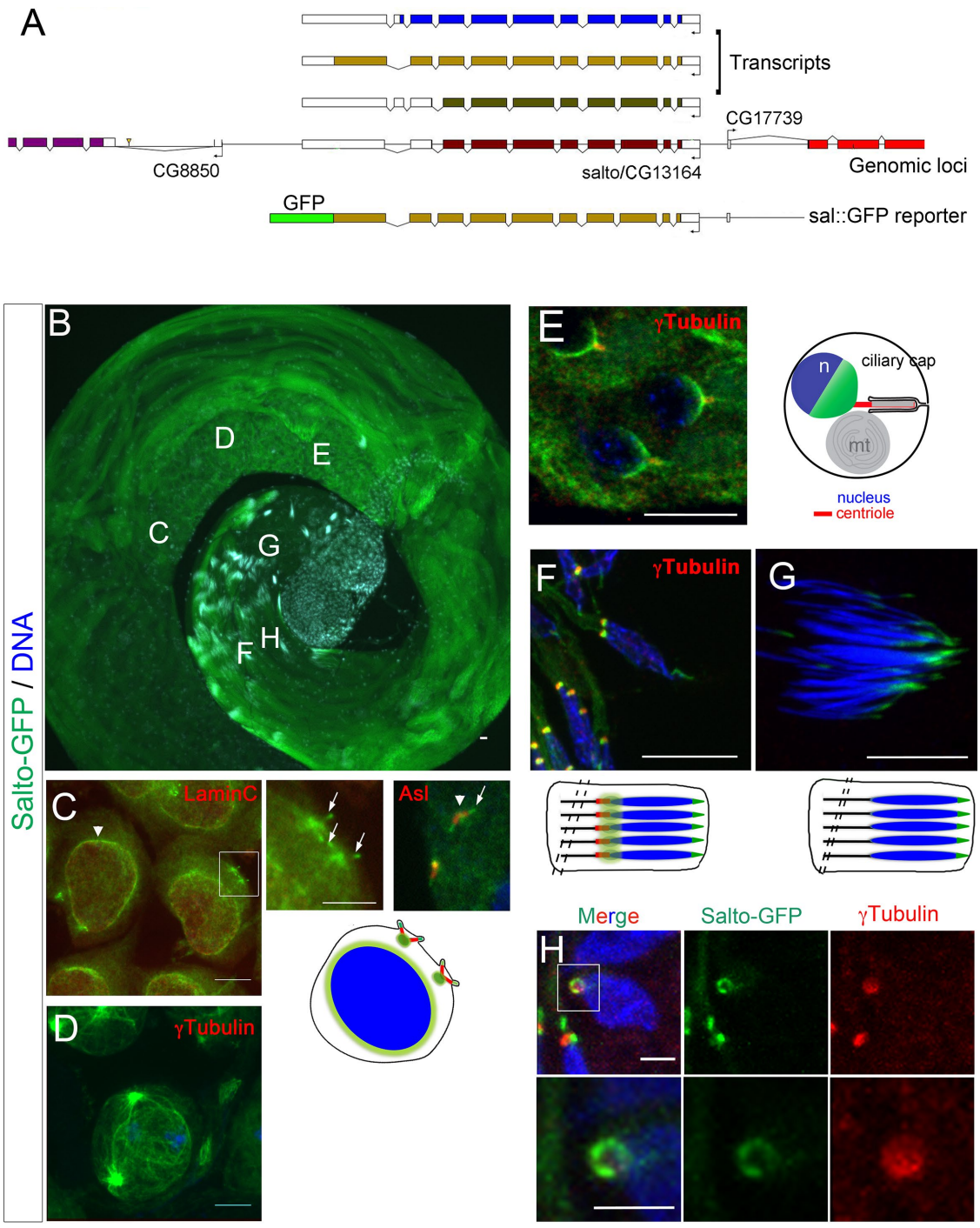

FIGURE 1: Salto–GFP is dynamically distributed during spermatogenesis. (A) Scheme of the *salto* locus and of its different transcripts. (B) Whole testis showing that Salto–GFP is present at all stages of spermatogenesis. (C) Spermatocytes express Salto–GFP around the centrioles and at the cilia/TZ (arrows). Salto–GFP is also located around the nuclei (arrowhead). A threefold magnification of the inset (white box) is shown in the middle panel. The right panel shows a representative spermatocyte with centrioles labeled with an anti-Asterless antibody (red); Salto–GFP is found both at the tip of the centrioles (arrow) and around the base (arrowhead). The scheme under the panel represents Salto–GFP localization in spermatocytes in green, nuclei in blue, and centrioles in red. (D) Before the beginning of meiosis, Salto also decorates the spindle poles and microtubules. (E) In round spermatids, Salto–GFP is present as a half ring around the nuclei and surrounds the centriole labeled by γ-tubulin antibody. (F) In late elongated spermatids, Salto–GFP is present both at the acrosome and at the centriolar adjunct. (G) Salto–GFP remains at the acrosome in later stages. Schemes underneath represent Salto–GFP localization in spermatids. B–G, scale bars = 10 μm. (H) Salto–GFP (green) is localized at the centriolar adjunct (labeled by γ-tubulin antibody, red) that forms a ring at the base of the centriole, where it is anchored in the nucleus (blue). Bottom panels are 2.2-fold magnification of the inset shown in the top panel. Scale bars = 2 μm.

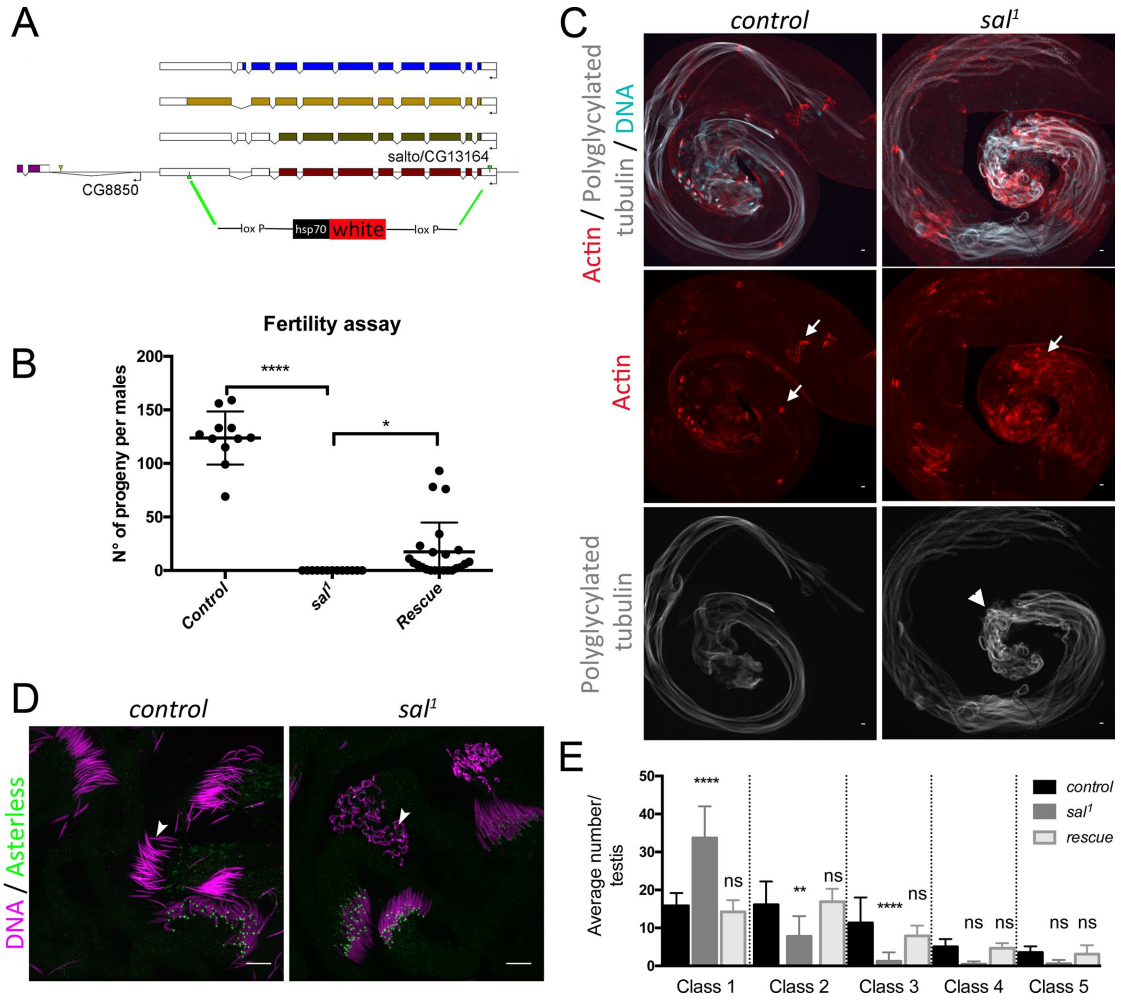

FIGURE 2: *sal*^{1} null mutant males are sterile and show sperm individualization defects. (A) The mini-white gene was inserted into the *salto* locus by CRISPR-Cas9–induced homologous recombination, eliminating all *salto* coding sequences. (B) Graph of fertility assays representing the number of progeny for control, rescue, and *sal*^{1} mutant males ($n = 11, 13, 25$, males respectively). (C) Whole testes labeled for polyglycylated tubulin (gray) and actin (red). Investment cone (IC) migration is altered in *sal*^{1} mutant testes compared with controls. Whereas IC (arrows) are clustered and regularly organized in wild-type testes, their distribution is dispersed in *sal*^{1} mutant testes. The spermatid tails are aberrantly coiled (arrowhead) in the proximal part of the *sal*^{1} mutant testes. (D) Images showing coiled nuclei (Hoechst in magenta) in *sal*^{1} mutant (arrowhead) compare to the long needle-shaped nuclei in control testes (arrowhead). Centrioles are labeled with asterless antibody (green). Scale bars = 10 µm. (E) Quantifications of the status of the nuclei and investment cones (IC) in control ($n = 10$), *sal*^{1} ($n = 9$), or rescue ($n = 9$) testes. Class 1 represents elongated nuclei before IC formation, class 2 is nuclei with assembled IC, class 3 is nuclei with IC starting to migrate, class 4 is migrating IC, and class 5 is disassembling IC in waste bags (see Supplemental Figure S4 for representative images of the categories). Results are presented as average numbers of events observed in testes. Statistical analysis was performed using ANOVA with multiple pairwise comparisons. In each class, statistical significance of variations relative to controls is indicated.

introducing two copies of a *salto::GFP*–expressing transgene (Figure 2B). This incomplete rescue could be explained either by functional interference of the GFP coding sequence or by reduced Salto–GFP production levels, as even though *salto–GFP* expression is under the control of the *salto* promoter, the rescue construct lacks the *sal* 3′UTR that could be needed to reproduce the full expression characteristics.

Because we observed no mature sperm in the seminal vesicles of *sal*^{1} mutant males (unpublished data), we looked at their testis organization. Detection of polyglycylated tubulin showed normal elongation, but increased tail coiling of late spermatids inside the testis (Figure 2C). This is suggestive of individualization defects. Individualization requires the formation of investment cones (IC), composed in particular of F-actin (Steinhauer, 2015), which can be detected using fluorescent phalloidin (Figure 2C). Whereas IC were apparently correctly forming at the base of the clustered nuclei, only a few progressing IC could be observed in *sal*^{1} mutant testes (Figure 2C). Strikingly, we observed that nuclei were not properly shaped in late elongated spermatids. Instead of forming long needles, they appeared coiled and twisted (Figure 2D).

To determine whether the sperm tail was correctly formed, we performed an ultrastructural analysis of transverse sections of mutant testes. No ultrastructural defects of the axoneme could be detected (Supplemental Figure S3). However, we observed abnormal morphologies of the mitochondrial derivatives on transverse sections of the spermatids (Supplemental Figure S3). The major derivative often appeared elongated (Supplemental Figure S3) relative to the round mitochondrial derivatives in control testes.

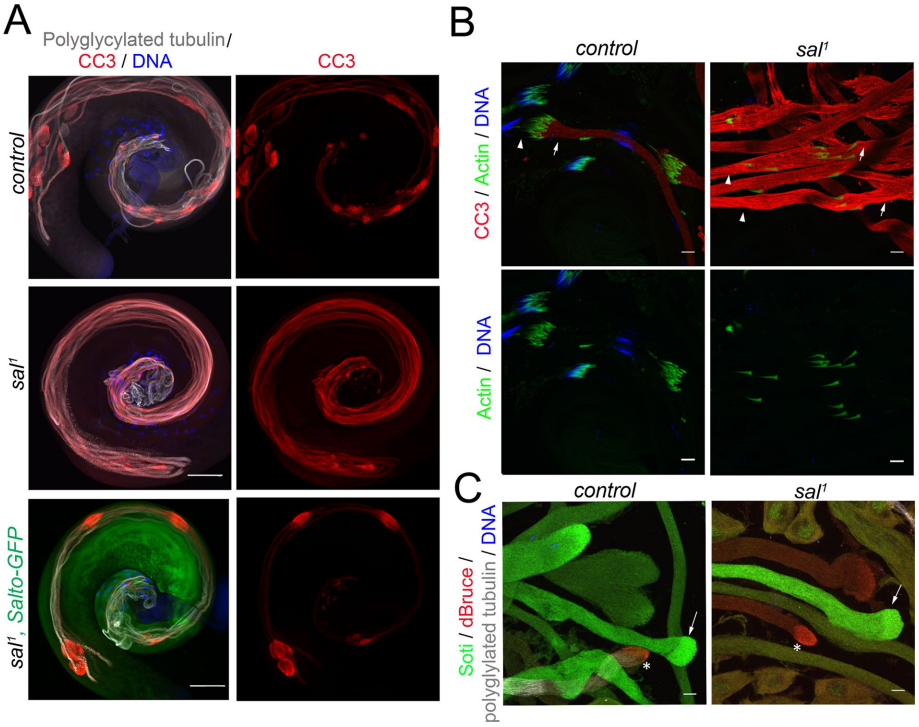

FIGURE 3: *salto* mutant spermatids exhibit individualization defects with elevated levels of active caspase 3. (A) Testes from wild type, *sal*^{1} mutant, and *sal*^{1} rescued with two copies of *salto::GFP* were stained with anti-cleaved caspase 3 antibody (CC3, red), polyglycylated tubulin (gray), and Hoechst to visualize the nuclei (blue). The red channel is shown alone on the right. Scale bar = 100 µm. (B) Squashed testes stained for cleaved caspase 3 (CC3, red), actin (green), and nuclei (blue) showing the postindividualized (arrowhead) and preindividualized (arrow) segments of the spermatids. In *sal*^{1} mutants, caspase 3 is active both before (arrowheads) and after (arrows) the IC. Bottom panels show the altered IC distribution in *sal*^{1} testes compared with controls. (C) Visualization of Soti (green) and dBruce (red) proteins at the spermatid tips (arrows and asterisks, respectively) both in controls and in *sal*^{1} mutants. Scale bars = 10 µm.

Individualization defects are associated with stalled IC

We quantified the efficiency of IC formation and migration by counting the IC at different steps of progression along the testis, either just assembling (class 2), starting to migrate (class 3), progressing along the testis (class 4), or finally disassembling in the waste bag (class 5). We observed that a larger number of nuclei are not associated with IC (class I) and most IC fail to migrate along the testis in *sal*^{1} testes compared with controls (Figure 2E). IC distribution is fully restored in rescued testes. This clearly indicates that Salto is required for IC assembly and progression. To understand the individualization defects, we also addressed the organization of the ICs. Actin detection by phalloidin showed that ICs form on the nuclei just at the onset of coiling (Supplemental Figure S4A), but disconnect from the curled nuclei and do not migrate. Jar, a myosin VI orthologue, is essential for IC migration and locates at the base of the actin cones (Rogat and Miller, 2002) from the onset of IC migration and all through their migration. We observed that in *sal*^{1} testes, Jar motor protein is localized, as in control flies, at the base of the ICs despite their altered distribution and migration (Supplemental Figure S4B). Hence, *sal*^{1} is not essential for the recruitment of Jar at the leading edge of ICs.

Spermatid individualization also involves nonapoptotic caspase activation. We determined whether caspase activation could be affected in *sal*^{1} mutants. In wild-type cysts, a gradient of active caspase 3 is induced, progressively decreasing from the cystic bulge formed by migrating IC toward the distal end of the flagella (Figure 3A). During IC progression, active caspase is removed from postindividualized spermatid ends. Hence, active caspase 3 is found only distal to the migrating actin cones. We observed that *sal*^{1} mutants display elevated levels of active caspase 3 all along the spermatid cysts (Figure 3, A and B). Cystic bulges are barely formed in comparison with controls (Figure 3, A and B), and even in cysts with migrating ICs, activated caspase 3 is observed both proximal and distal to migrating IC (Figure 3B). This indicates that migrating ICs are ineffective in creating cystic bulges and hence in removing active caspase 3 and cytoplasm in *sal*^{1} testes. This phenotype is rescued by adding two copies of *sal::GFP* transgene (Figure 3A). To check that elevated levels of active caspase are not due to defects in the distribution of caspase inhibitors, we looked for the localization of Soti and dBruce, two inhibitors of the Cullin complex (Kaplan *et al.*, 2010). These inhibitors form two successive gradients of expression, increasing from the nucleus to the caudal flagellar tip in control testes. In *sal*^{1}, both proteins are distributed as in controls (Figure 3C).

Hence, our results indicate that sperm individualization defects are likely due to impaired or inefficient IC migration and not altered regulation of the caspase pathway.

Salto is required for sperm nuclear shaping

The most striking defects of *sal*^{1} mutants is the coiling of the nuclei at late stages of differentiation. We first determined the precise onset of nuclear coiling. We observed that coiling only takes place after the beginning of actin recruitment before complete assembly of the actin cones (Figure 4A).

We checked whether nuclear shaping defects could be associated with altered chromatin remodeling. We did not observe any recruitment defects of Tpl94D, a transition protein incorporated at the histone to protamine transition, nor of the protamine protein Mst35Bb (Rathke *et al.*, 2007). Both are incorporated in *sal*^{1} nuclei as in controls (Figure 4B). By EM, we looked at the structure of the DC and the associated nucleus during spermatid differentiation. We did not observe obvious defects of the DC nor of the fenestrated nuclear membrane. The microtubules of the DC cluster on one side of the nucleus in *sal*^{1} testes and mark nucleus invagination during head elongation (Figure 4C), indicating that nucleus invagination is initiated properly. We only observed variability in the size and shape of the centriolar adjunct that surrounds the basal body. This variability was not observed in control testes (Figure 4D). Also, the nuclear membrane appeared more tortuous in *sal*^{1} testes than in controls, in which the nuclear membrane appears smoother (Figure 4E, arrowheads in top panels for intermediate spermatid stages; arrows in bottom panels for late stages).

We thus addressed whether we could observe functional alterations of known DC components. Several proteins have been described as involved in DC homeostasis in *Drosophila* (Kracklauer *et al.*, 2010; Texada *et al.*, 2011; Sitaram *et al.*, 2012). Spag4 is a SUN domain containing protein associated with the DC of spermatids in *Drosophila*. At all maturation steps, there was no alteration

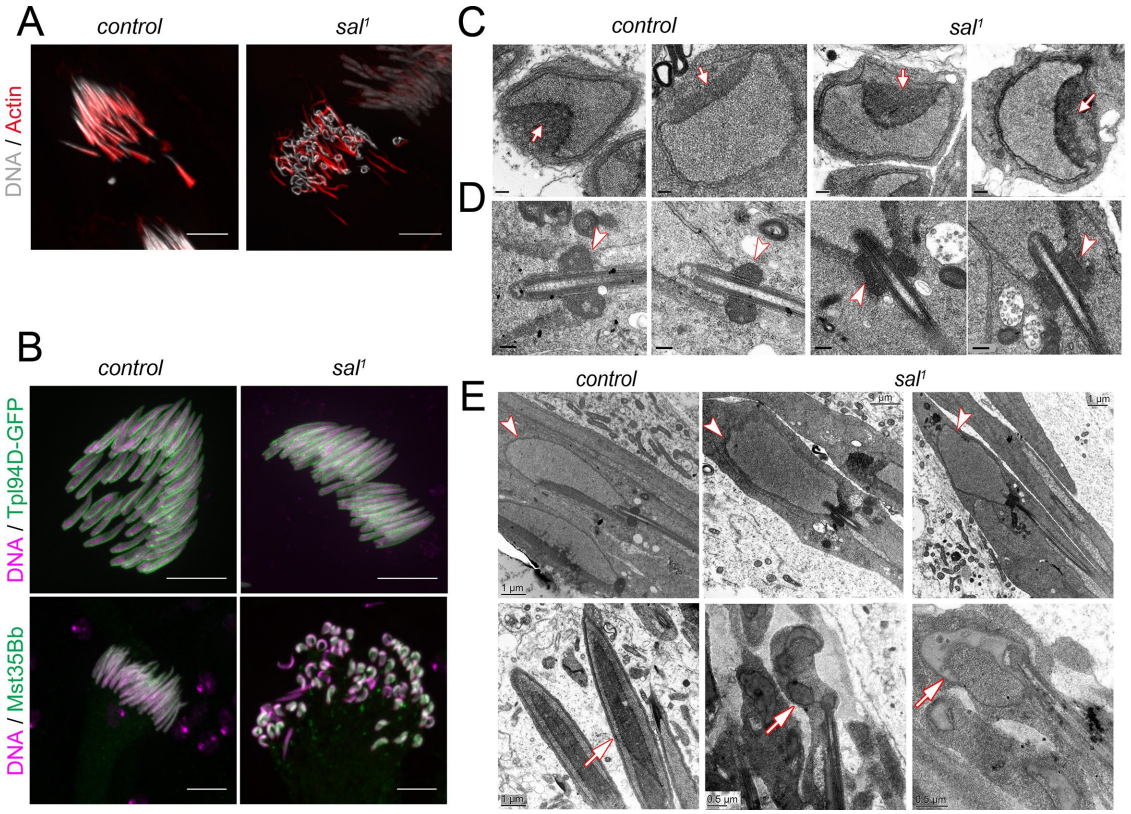

FIGURE 4: Salto is required for sperm nuclear shaping. (A) Nuclei (white) are coiling at the onset of IC assembly (red) as stained with Hoechst. (B) Transition protein Tpl94D (top panels in green) and protamine Mst35Bb (bottom panels in green) are correctly incorporated into the nuclei (magenta) of both control and *sal*^{1} mutant spermatids. Scale bars = 10 µm. (C) EM sections of sperm heads showing the microtubules of the dense complex (arrows) present on the invaginated side of the nucleus. No differences in the apparent organization of the microtubule network could be observed. Scale bars = 200 nm. (D) EM sections of the centriolar adjunct (arrowhead), which appears irregular in shape and size in *sal*^{1} mutant testes compared with controls. Scale bars = 200 nm. (E) EM sections of nuclei. At intermediate stages and before coiling (top panels), *sal*^{1} nuclei have a rougher membrane (arrowhead) than control nuclei. At late stages (bottom panels), bending of *sal*^{1} mutant nuclei compared with controls is indicated by white arrows.

of Spag4 localization in *salto* mutants (Figure 5A). As well, Lis1 is a dynein-associated protein involved in the localization of dynein around the nuclei (Sitaram *et al.*, 2012) and is properly located in *sal*^{1} spermatids (Figure 5B). Two other unrelated proteins, CG4329 and CG12184, that we have characterized as being localized at the dense complex (J.A.L., unpublished results), are also properly distributed in *sal*^{1} mutants (Figure 5B). These results indicate that Salto is not required for the localization of these other components associated with the dense complex in *Drosophila*.

However, using these cell markers, we observed, on a few occasions, defects of basal body–to–nucleus attachment in *sal*^{1} round spermatids (Figure 5, B and C). Such defects are also observed in *spag4* mutant spermatids. Indeed, previously described null mutants for *spag4* show phenotypes strikingly similar to *sal*^{1} in the testes, with identical individualization and nuclear-shaping defects (Texada *et al.*, 2008; Kracklauer *et al.*, 2010). We hence looked at the distribution of Salto in the previously described null *spag4*^{6} mutant flies (Kracklauer *et al.*, 2010), but we did not observe any defects (Figure 5D), indicating that Salto and Spag4 localization do not rely on each other. Interestingly, we noticed that in addition to previously described phenotypes, *spag4*^{6} mutant flies show elevated caspase 3 activation (Figure 5E), with no cystic bulge or waste bags, as described above in the *sal*^{1} mutant, supporting the hypothesis that both genes are involved in the same biological process. We thus investigated possible genetic interactions between *salto* and *spag4*. In *sal*^{1}*/+; spag4*^{6}*/+* trans heterozygotes, fly fertility was not affected and we observed properly formed nuclei and basal body anchoring. The homozygote *sal*^{1}, *spag4*^{6} mutants show defects similar to those in *spag4*^{6}, indicating that *spag4* and *salto* do not have additive or synergistic actions and thus are likely to work in the same pathway. Altogether, our results indicate that *salto* and *spag4* act in the genetic pathway involved in sperm nuclear shaping and tail-to-nucleus attachment during *Drosophila* spermiogenesis.

DISCUSSION

Our results show that *salto* encodes a dynamically located protein with centriolar associated components, the dense body, equivalent to the mammalian nuclear manchette, and the acrosome during spermatogenesis. In agreement with this localization, *sal*^{1} mutants do not exhibit developmental defects, but grow normally, and their only phenotype is male sterility characterized by individualization and sperm head morphogenesis defects.

Both cellular phenotypes were fully rescued by expressing the Salto–GFP fusion protein, even though male fertility was not fully restored. This suggests that reduced fertility of the rescued *sal*^{1} mutant is not linked to the function of Salto in sperm-head shaping and sperm individualization, but could rely on other possible functions of Salto in sperm differentiation that our observations did not reveal.

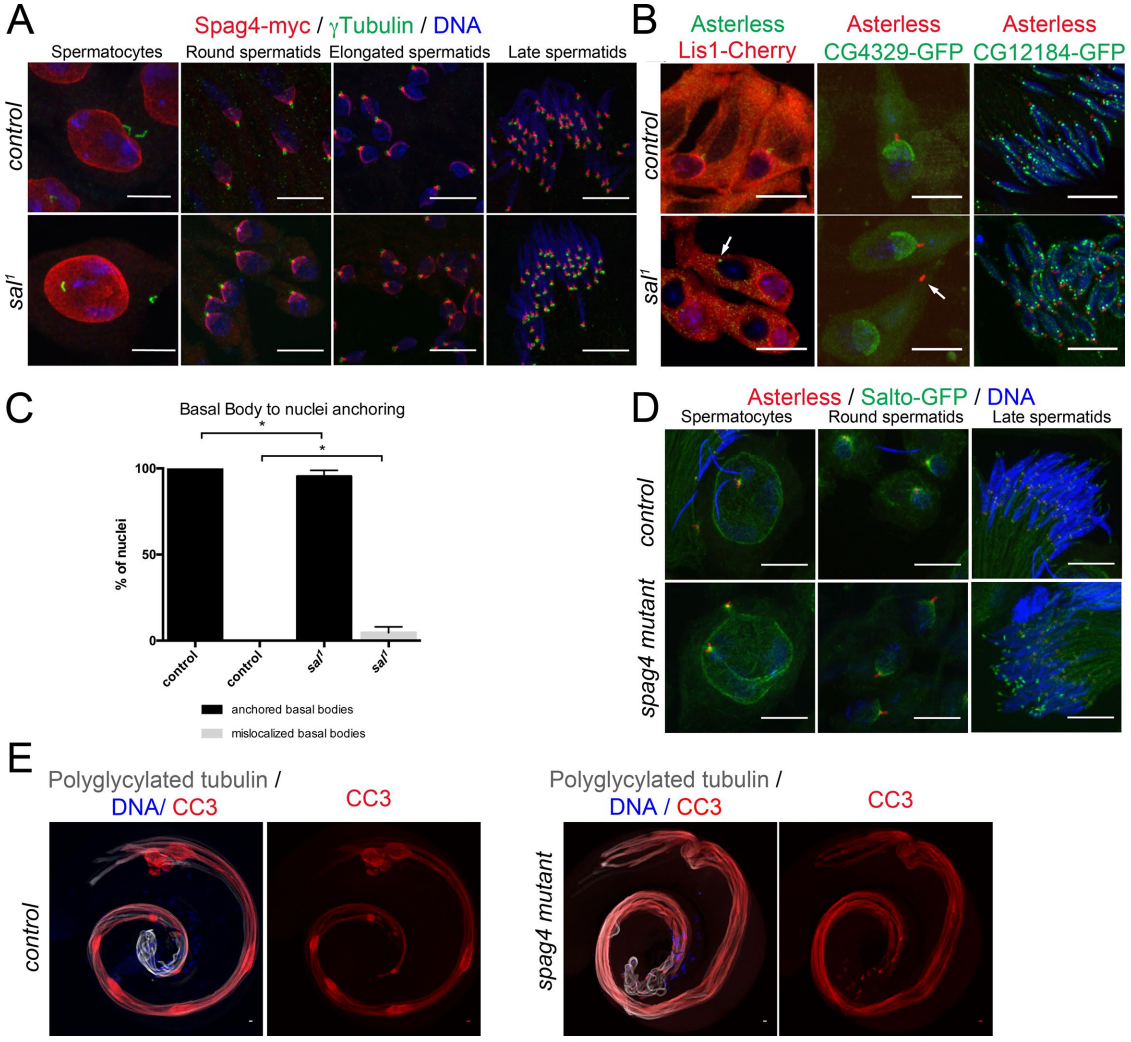

FIGURE 5: *salto* and *spag4* functional relationships. (A) Spag4-myc localization in *sal*^{1} mutants during spermatogenesis. Centrioles are stained with γ-tubulin antibody in green and nuclei (Hoechst, in blue). Spag4 is correctly located around the nuclei in spermatocytes and at the dense complex in round and elongated spermatids. It is relocated at the centriolar adjunct in late spermatids. (B) Images of dense complex components: Lis1 (first panels in red), CG4329 (second panels in green), and CG12184 (third panels in green) in controls and *sal*^{1} mutants. Basal bodies (Asterless respectively in green or red) are on rare occasions undocked to the nuclei in *sal*^{1} mutant spermatids (arrows). (C) Quantification of basal body attachment defects in *sal*^{1} early elongating spermatids (n = 100 for controls and 96 for *sal*^{1}). (D) Salto–GFP localization in *spag4* mutant during spermatogenesis. Salto–GFP is similarly located at all steps of maturation in control or in *spag4* mutant spermatids. (E) *spag4* mutant spermatids exhibit elevated caspase levels (red) compared with controls. Scale bars = 10 μm.

The Salto C-terminus was isolated in a yeast two-hybrid screen with full-length Cby as bait, and Salto can be found in the same compartment as Cby at the transition zone (Enjolras *et al.*, 2012; Vieillard *et al.*, 2016). However, Cby distribution is not affected in *sal*^{1} mutants, and as well, Salto–GFP distribution is not affected in *cby*^{1} testes (unpublished data). In addition, *sal*^{1} and *cby* null mutants show completely different phenotypes (Enjolras *et al.*, 2012; Vieillard *et al.*, 2016), indicating that Cby and Salto exert their apparent functions in different pathways.

Salto is required for sperm-head morphogenesis

The most striking defect in *sal*^{1} mutant males is the abnormal coiling of the nuclei. It is important to note that even though we did not fully restore male fertility, nuclear coiling defects were fully rescued by expressing Salto–GFP. Nuclear shaping defects could originate from different impaired pathways. Based on Salto distribution, Salto could be required for proper manchette action to shape the sperm head. Indeed, Salto distribution reflects the microtubule network that cages the nuclei and forms the dense complex. Salto could be required for the integrity of the microtubule network of the sperm manchette. However, using immunofluorescence (unpublished data) or electron microscopy (EM) analysis, we did not identify defects of the microtubule network around the nuclei, nor of other components known to be associated with the dense complex in *Drosophila*. Therefore, we expect Salto to play a role downstream or parallel to the organization of the microtubule network. Salto possibly harbors a BAR domain, known to be involved in lipid membrane association, and thus Salto could participate in linking the microtubule network to membrane domains (Stanishneva-Konovalova *et al.*, 2016). In agreement with this hypothesis, mutation of the Spag4 protein, which is a

nuclear–inner membrane protein, leads to nuclear shaping defects similar to those with *sal*^{1} (Kracklauer *et al*., 2010) indicating that the tight association of the nuclear membrane to the microtubule network is required for nuclear shaping. Salto could also be involved in the active transport that takes place along sperm manchette microtubules during nuclear reshaping.

It is important to note that Salto is also present at the acrosome during spermatid elongation steps. The incomplete rescue of *sal*^{1} fertility could be due to improper function of Sal–GFP at the acrosome which is required for fertility. In humans, defects in acrosome formation are associated with globozoospermia, characterized by abnormal round spermatid heads (Ray *et al*., 2017). How acrosome defects contribute to the abnormal shaping of the nuclei is not completely understood. Polarized transport along microtubules is a likely common pathway involved in acrosome and nuclear shaping defects. Among the genes responsible for globozoospermia in humans, the kinesin 14 KIFC1 plays a role in organizing microtubule-associated transport (Zhi *et al*., 2016). In the lobster, mutations of the orthologue KifC1 induce acrosome malformation and nuclear shaping defects (Ma *et al*., 2017). In this context, Salto could be involved in microtubule-associated transport, implicated in both acrosome formation and manchette function. The acrosome could be an anchoring platform for microtubules and therefore contribute to normal nuclear shaping. As Salto is also present both at the centriolar adjunct and at the acrosome, it could also be required for linking the microtubule network to both ends of the nuclei. In the absence of Salto, these links would be weakened and the nuclei would coil under the mechanical constraints imposed by microtubule rearrangements. Further work is needed to identify more precisely the partners of Salto during nuclear shaping and to understand how they are involved in this process.

Salto is involved in basal body and centriolar adjunct homeostasis

In the *sal*^{1} mutant, we observed a significant but scarcely penetrant defect in basal body anchoring into the nuclei at the round spermatid stage (4% of cells clearly showed this defect). This indicates that Salto is not essential for basal body anchoring but could play a redundant function with other, yet to be identified, genes required for nuclear basal body anchoring. Strikingly, *spag4* mutant spermatids show basal body anchoring defects associated with nuclear coiling as *sal*^{1} mutants. We did not identify genetic interactions in the nuclear anchoring function between *salto* and *spag4,* as the double heterozygous mutants show no anchoring defects and double homozygous mutants are similar to *spag4* mutants (unpublished data). However, this suggests that Salto could act, like Spag4, to connect the nuclear membrane to the cytoskeleton network. In support of a function of Salto in basal body nuclear anchoring, we observed, by EM, shape variability of the centriolar adjunct, indicating that Salto is needed to organize the basal body/nuclear interface.

Interestingly, the angiotensin-converting enzyme (Ance) is a peptidyl dipeptidase implicated in male fertility. *Ance* mutants present a defect in nuclear morphology similar to those observed in *sal*^{1}. *Ance* mutant spermatids also show mitochondrial defects, the major and the minor derivatives being misshapen compared with control spermatids (Hurst *et al*., 2003). We observed similar misshaping of the major mitochondria derivative in *sal1* mutants (Supplemental Figure S3), suggesting that Ance and Salto could be involved in convergent pathways. Further studies are required to understand the molecular links between nuclear shaping, basal body anchoring, and mitochondria morphogenesis, but Salto appears to be an important player in these processes.

Origin of the individualization defects in *sal*^{1} mutants

Individualization defects can be a consequence of various impaired pathways (Steinhauer, 2015). We have excluded several of the possible causes, as we did not observe axonemal defects (Supplemental Figure S3) or misorganization of the formation of the IC (Supplemental Figure S4). Defects in individualization can also be a consequence of impaired caspase activation (Arama *et al*., 2007; Fabian and Brill, 2012). During IC progression, activated caspase forms a gradient from the cystic bulge to the distal cyst tail. We determined that *salto* mutants present an elevated level of activated caspase from head to tail. We did not observe any distribution defects of the regulators of the caspase pathway, Soti or dBruce, indicating that elevated caspase 3 activation is not associated with reduced levels of inhibition. Because *salto* and *spag4* null mutants show similar profiles of caspase 3 activation, it is likely that this defect is a direct consequence of impaired actin cone progression. Alternatively, mitochondria are directly involved in regulating caspase 3 activation during spermatid individualization, as regulation of caspase 3 activation has been shown to be restricted in the mitochondrial vicinity by a protein (succinyl-CoA synthetase [SCS] b-subunit [A-Sb]) of the mitochondrial outer membrane (Aram *et al*., 2016). Hence, it is also plausible that the mitochondria-shaping defects observed in *sal*^{1} mutants could be responsible for caspase overactivation.

Nevertheless, individualization defects most likely originate directly from impaired manchette organization and nuclear coiling. Indeed, analysis of mutants for *salto*, *spag4*, and *yuri* and also of the proteasomal subunit *prosα6T* indicates that coiling of elongated nuclei is always correlated with failed IC progression (Zhong and Belote, 2007; Kracklauer *et al*., 2010; Texada *et al*., 2011). We observed that nuclear coiling appears after the onset of IC formation in *sal*^{1} mutants. The signals that trigger IC formation and progression are unknown, but these observations suggest that proteins associated with the sperm manchette/dense complex/centriolar adjunct are all required for IC progression. Altogether, this supports the conclusion of a tight association between sperm manchette organization and IC progression.

In conclusion, we show that Salto plays a critical role in organizing the sperm head. The similarities between spermatid individualization processes and nuclear shaping in *Drosophila* and mammals suggest that further studies of sperm differentiation in *Drosophila* may provide new insights into the etiology of some forms of human infertility.

MATERIALS AND METHODS

Fly stocks and maintenance

The following lines were obtained from Bloomington *Drosophila* Stock Center: *vasa::Cas9* (Bl#51323); *spag4* mutant: w[*];TI{w[+mW.hs] = TI}spag4^{6}/CyO (Bl#29978); reporter gene *Spag4::Myc*: w[*]; P{w[+mC] = spag4.6xMyc}3/TM6B, Tb[1] (Bl#29981); deficiency that covers the *salto* locus (Bl#24967); *Lis1::cherry* for dense complex marker (Bl#57339). For controls, we used *w*^{1118} flies to compare background fluorescence intensity with Salto–GFP. *w*^{1118}; *sal*^{1}*/Cyo* were used as controls to compare with *sal*^{1} mutant phenotypes. The flies were raised on standard media between 21° and 25°C.

Yeast two-hybrid screen

Total RNA from wild-type *Drosophila* testis was extracted using TRIzol reagent (Thermo Fisher Scientific). A testis-specific cDNA library was constructed by Hybrigenics, who further performed a yeast two-hybrid screen using Cby as bait.

Generation of *sal*^{1} allele

The *sal*^{1} allele (CG13164) was generated by CRISPR/Cas9-induced homologous directed repair (Gratz *et al.*, 2014). Two guide RNAs (gRNAs) were selected using the http://tools.flycrispr.molbio.wisc.edu/targetFinder/website: 5′-CCATTTACACTAGACGTAGTTCA-3′ and 5′-CCGTCGAGCAGTTGATGCTGCAG-3′ (protospacer-adjacent motifs are underlined). Oligos were phosphorylated by T4PNK (New England Biolabs) and annealed. Double-stranded 5′ gRNA and 3′ gRNA were cloned in the *Bbs*I sites of pBFv-U6.2 and pBFv-U6.2B vectors, respectively (Kondo and Ueda, 2013). 5′ gRNA was further subcloned in the *Eco*RI–*Not*I sites of pBFv-U6.2B to express the two gRNAs from one vector. The 1.5 kb 5′ homologous arm was amplified by PCR with

Forward (F)-1 5′-TAATTCGCTAGCGTATTCTCGACAAGATTTGG-3′

Reverse (R)-2 5′-TAATTCCGTACGTGGTACAAAAATGCTTTCTG-3′.

The 1.5 kb 3′ homologous arm was amplified by PCR with

F-3 5′-TAATTAGATCTCGGCTTAATTCGCCCCGC-3′

R-4 5′-TAATTCCCTAGGAGTTGGTCAACAATGTTAGG-3′.

The resulting 5′ and 3′ homology arms were cloned into the *Bsi*WI–*Nhe*I and *Avr*II–*Bgl*II sites, respectively, of pJT38 (pRK2 plasmid [Huang *et al.*, 2008], with an attB cassette). The two vectors (gRNAs and homology arms) were injected into *vasa::Cas9* embryos. Flies were crossed to w; Bl/CyO virgin females, and the offspring were screened for red-eyed flies. Homologous recombination was checked by PCR.

Generation of Salto and of CG4329 and CG12184 GFP-expressing transgenes

For each gene, the entire coding sequence and at least 1 kb of upstream regulatory sequences were cloned in frame with GFP in the pJT61 vector (Vieillard *et al.*, 2016). Integration platforms and primers used were for *salto::GFP* (89E11[III])

F-5 5′-CGAAGTTATGCTAGCGGATCCTAATTGTCTTAATTATCCGCATTG-3′ and R-6 5′-GAATTAGCGGCCGCGAAATGGCGGGGCGAATT-3′;

for *CG4329::GFP* (89E11[III])

F-7 5′-TAATTCGCGGCCGCCGATTCTGATTTGCGCAAT-3′; R-8 5′-TAATTCGCGGCCGCCGATTCTGATTTGCGCAAT-3′;

for *CG12184::GFP* (53B2[II]), 2 PCR fragments of 2.5 kb with regulatory and coding sequence were cloned into pJT61 using a GIBSON assembly cloning kit (NEB):

F-9 5′-ATTGGGAATTCGTTAACAGATCTACCACTCATCAGTACGATG-3′; R-10 5′-GCGCTGTTTAGCTTTCCTTTGGTCTCTCATGAGTGGC-3′; F-11 5′-GGGAGCAGCAAGAAATTCAGCCACTCATGAGAGACC-3′; R-12 5′-CGAGCCGCGGCCGCAGATCTTCGATCTTCTCTAGATGATTAC-3′.

The resulting constructs were integrated by PhiC31-mediated recombination at attB platforms. All transgenic lines were obtained from BestGene.

Immunofluorescence on *Drosophila* testes squashes

Testes from young adult flies (between 0 and 2 d old) were dissected in phosphate-buffered saline (PBS)1X and fixed 15 min in PBS1X/paraformaldehyde 4%. For squash preparation, testes were squashed between coverslip and slide and frozen in liquid nitrogen. The coverslip was removed, and the slide was soaked for 2 min in ethanol 100% at –20°C. For both whole testis and squash immunofluorescence, testes were permeabilized 15 min in PBS1X/Triton 0.1% (PBT) and blocked 2 h in PBT/bovine serum albumin 3%/normal goat serum 5%.

Primary antibodies were incubated in blocking buffer overnight at 4°C. Fixed testes were then washed in PBS1X and incubated 2 h in secondary Alexa Fluor antibodies diluted in PBS1X. Slides were washed in PBS1X and rinsed in ultrapure water. Slides were mounted using Vectashield containing Hoechst (1:1000). Antibodies used were the following: guinea pig anti-Asterless (1/30,000; gift from C. Rogers, University of Arizona, Tucson, AZ; Klebba *et al.*, 2013); mouse Axo49 anti–polyglycylated tubulin (1/100; provided by N. Levilliers, Laboratoire de Biologie Cellulaire 4, CNRS, Université Paris-Sud, Orsay, France); rabbit anti-Tpl94D (1/100) and Mst35Bb (1/200) kindly provided by B. Loppin, LBBE, CNRS UMR 5558 (Kimura and Loppin, 2016); mouse anti–alpha-tubulin DM1a (1/500) (Sigma Aldrich); mouse anti-Myosin VI/jaguar (1/200) (Kellerman and Miller, 1992), kindly provided by Stéphane Vincent (ENSL); rabbit anti-cleaved caspase 3 (CC3) (1/100) (Cell Signaling); guinea pig anti-Soti (1/100) and rabbit anti-dBruce (1/500, kindly provided by E. Arama); mouse anti-LaminC (1/25) (DHSB).

For colcemid treatments, testes were incubated 1 h in 10 µM colcemid before being processed as above.

Most slides were imaged using an IX83 microscope from Olympus equipped with an iXon Ultra 888 EMCDD camera from Andor and IQ3 software from Andor. A PlanApo N Apochromat 10× or a 60 × 1.42NA objective from Olympus was used for all acquisitions.

All images were processed with ImageJ. Figures were created with Adobe Photoshop. Only contrasts and offset were adjusted.

Fertility test

One or 2 d–old males were crossed individually with two w^{1118} virgin females. After 5 d, crosses with at least one dead fly were eliminated from the test. Mated flies were discarded from conserved crosses. All flies that hatched out from the crosses were counted.

EM

Samples were processed as described previously (Enjolras *et al.* 2012; Vieillard *et al.* 2016).

Sequence alignment

Protein sequences were obtained from the National Center for Biotechnology Information (NCBI). We identified orthologues for Salto/CG13164 (NCBI protein accession number AAF58537) in Drosophilidae: *D. simulans*, GD25850 (KMY93149); *D. yakuba*, GE13459 (EDW90806); *D. erecta*, GG22589 (EDV56349); *D. sechellia*, GM20369 (EDW47532); and in the bilateria *C. savignyi,* Uniprot accession number H2YNR4 using orthoDB v9.1 (Zdobnov *et al.*, 2017). Protein with a similar SMN domain were also found in other arthropods: *Hyalella azteca* (accession n° XP_018027323.1), *Cyphomyrmex costatus* (accession n° XP_018402034.1), and *Amyelois transitella* (accession n° XP_013184881.1).

Alignment was produced using PRALINE (PSI-BLAST; Simossis and Heringa, 2005).

A tree was made using the distance method on Seaview v4.7 software (Gouy *et al.*, 2010).

Quantification and statistics

For basal bodies–to–nuclei anchoring, we used CG4329–GFP to visualize the half ring of microtubules around the nuclei (stained with Hoechst) and labeled centrioles with γ-tubulin antibody. The

centrioles nonanchored to the nuclei were counted on round spermatids. The experiment was repeated four times and 20–25 cells were counted for each.

Results are represented as scatterplots with the mean and SD on all figures. For Figures 2B and 5C, statistical significance was determined by a two-tailed unpaired Student's *t* test. For Figure 2E, statistical significance was determined using analysis of variance (ANOVA) with multiple pairwise comparisons. (Prism 6 software; ns, $p > 0.05$; *, $p \leq 0.05$; **, $p \leq 0.01$; ***, $p \leq 0.001$; ****, $p \leq 0.0001$.)

ACKNOWLEDGMENTS

We thank M. NGassa for help in IC complex quantifications. We thank E. Arama for providing dBruce and Soti antibody. EM observations were performed at the CTμ (University Lyon 1). This project was supported by a grant from the Fondation pour la Recherche Médicale, FRM DEQ20131029168, and the Agence Nationale de la Recherche (ANR Divercil). C.A. was supported by a PhD fellowship from the University Claude Bernard Lyon-1. J.A.L. was supported by FRM DEQ20131029168.

REFERENCES

Aram L, Braun T, Braverman C, Kaplan Y, Ravid L, Levin-Zaidman S, Arama E (2016). A Krebs cycle component limits caspase activation rate through mitochondrial surface restriction of CRL activation. Dev Cell 37, 15–33.

Arama E, Bader M, Rieckhof GE, Steller H (2007). A ubiquitin ligase complex regulates caspase activation during sperm differentiation in *Drosophila*. PLoS Biol 5, e251.

Brown JB, Boley N, Eisman R, May GE, Stoiber MH, Duff MO, Booth BW, Wen J, Park S, Suzuki AM, *et al*. (2014). Diversity and dynamics of the *Drosophila* transcriptome. Nature 512, 393–399.

Calvi A, Wong ASW, Wright G, Wong ESM, Loo TH, Stewart CL, Burke B (2015). SUN4 is essential for nuclear remodeling during mammalian spermiogenesis. Dev Biol 407, 321–330.

Enjolras C, Thomas J, Chhin B, Cortier E, Duteyrat JL, Soulavie F, Kernan MJ, Laurencon A, Durand B (2012). *Drosophila* chibby is required for basal body formation and ciliogenesis but not for Wg signaling. J Cell Biol 197, 313–325.

Fabian L, Brill JA (2012). *Drosophila* spermiogenesis: big things come from little packages. Spermatogenesis 2, 197–212.

Fabrizio J, Hime G, Lemmon S, Bazinet C (1998). Genetic dissection of sperm individualization in *Drosophila melanogaster*. Development 125, 1833–1843.

Geer LY, Domrachev M, Lipman DJ, Bryant SH (2002). CDART: protein homology by domain architecture. Genome Res 12, 1619–1623.

Gouy M, Guindon S, Gascuel O (2010). SeaView version 4: a multiplatform graphical user interface for sequence alignment and phylogenetic tree building. Mol Biol Evol 27, 221–224.

Gratz SJ, Ukken FP, Rubinstein CD, Thiede G, Donohue LK, Cummings AM, O'Connor-Giles KM (2014). Highly specific and efficient CRISPR/Cas9-catalyzed homology-directed repair in *Drosophila*. Genetics 196, 961–971.

Huang J, Zhou W, Watson AM, Jan Y-N, Hong Y (2008). Efficient ends-out gene targeting in *Drosophila*. Genetics 180, 703–707.

Hurst D, Rylett CM, Isaac RE, Shirras AD (2003). The *Drosophila* angiotensin-converting enzyme homologue Ance is required for spermiogenesis. Dev Biol 254, 238–247.

Kaplan Y, Gibbs-Bar L, Kalifa Y, Feinstein-Rotkopf Y, Arama E (2010). Gradients of a ubiquitin E3 ligase inhibitor and a caspase inhibitor determine differentiation or death in spermatids. Dev Cell 19, 160–173.

Keller LC, Geimer S, Romijn E, Yates J, Zamora I, Marshall WF (2009). Molecular architecture of the centriole proteome: the conserved WD40 domain protein POC1 is required for centriole duplication and length control. Mol Biol Cell 20, 1150–1166.

Kellerman KA, Miller KG (1992). An unconventional myosin heavy chain gene from *Drosophila melanogaster*. J Cell Biol 119, 823–834.

Kierszenbaum AL (2002). Intramanchette transport (IMT): managing the making of the spermatid head, centrosome, and tail. Mol Reprod Dev 63, 1–4.

Kimura S, Loppin B (2016). The *Drosophila* chromosomal protein Mst77F is processed to generate an essential component of mature sperm chromatin. Open Biol 6, 160207.

Klebba JE, Buster DW, Nguyen AL, Swatkoski S, Gucek M, Rusan NM, Rogers GC (2013). Polo-like kinase 4 autodestructs by generating its Slimb-binding phosphodegron. Curr Biol 23, 2255–2261.

Kondo S, Ueda R (2013). Highly improved gene targeting by germline-specific Cas9 expression in Drosophila. Genetics 195, 715–721.

Kracklauer MP, Wiora HM, Deery WJ, Chen X, Bolival B, Romanowicz D, Simonette RA, Fuller MT, Fischer JA, Beckingham KM (2010). The Drosophila SUN protein Spag4 cooperates with the coiled-coil protein Yuri Gagarin to maintain association of the basal body and spermatid nucleus. J Cell Sci 123, 2763–2772.

Lehti MS, Sironen A (2016). Formation and function of the manchette and flagellum during spermatogenesis. Reproduction 151, R43–R54.

Ma D-D, Bi L, Yang W-X (2017). KIFC1 is essential for acrosome formation and nuclear shaping during spermiogenesis in the lobster *Procambarus clarkii*. Oncotarget 8, 36082–36098.

Marchler-Bauer A, *et al*. (2017). CDD/SPARCLE: functional classification of proteins via subfamily domain architectures. Nucleic Acids Res 45, D200–D203.

Noguchi T (2003). A role for actin dynamics in individualization during spermatogenesis in *Drosophila melanogaster*. Development 130, 1805–1816.

O'Donnell L (2014). Mechanisms of spermiogenesis and spermiation and how they are disturbed. Spermatogenesis 4, e979623–11.

Pratt MB, Titlow JS, Davis I, Barker AR, Dawe HR, Raff JW, Roque H (2016). *Drosophila* sensory cilia lacking MKS proteins exhibit striking defects in development but only subtle defects in adults. J Cell Sci 129, 3732–3743.

Rathke C, Baarends WM, Jayaramaiah-Raja S, Bartkuhn M, Renkawitz R, Renkawitz-Pohl R (2007). Transition from a nucleosome-based to a protamine-based chromatin configuration during spermiogenesis in *Drosophila*. J Cell Sci 120, 1689–1700.

Ray PF, Touré A, Metzler-Guillemain C, Mitchell MJ, Arnoult C, Coutton C (2017). Genetic abnormalities leading to qualitative defects of sperm morphology or function. Clin Genet 91, 217–232.

Rogat AD, Miller KG (2002). A role for myosin VI in actin dynamics at sites of membrane remodeling during *Drosophila* spermatogenesis. J Cell Sci 115, 4855–4865.

Simossis VA, Heringa J (2005). PRALINE: a multiple sequence alignment toolbox that integrates homology-extended and secondary structure information. Nucleic Acids Res 33, W289–W294.

Sitaram P, Anderson MA, Jodoin JN, Lee E, Lee LA (2012). Regulation of dynein localization and centrosome positioning by Lis-1 and asunder during *Drosophila* spermatogenesis. Development 139, 2945–2954.

Stanishneva-Konovalova TB, Derkacheva NI, Polevova SV, Sokolova OS (2016). The role of BAR domain proteins in the regulation of membrane dynamics. Acta Naturae 8, 60–69.

Steinhauer J (2015). Separating from the pack: molecular mechanisms of *Drosophila* spermatid individualization. Spermatogenesis 5, e1041345.

Strunnikov AV, Jessberger R (1999). Structural maintenance of chromosomes (SMC) proteins: conserved molecular properties for multiple biological functions. Eur J Biochem 263, 6–13.

Texada M, Simonette R, Deery W, Beckingham K (2011). Tropomyosin is an interaction partner of the *Drosophila* coiled coil protein Yuri Gagarin. Exp Cell Res 317, 474–487.

Texada MJ, Simonette RA, Johnson CB, Deery WJ, Beckingham KM (2008). Yuri gagarin is required for actin, tubulin and basal body functions in *Drosophila* spermatogenesis. J Cell Sci 121, 1926–1936.

Vieillard J, Paschaki M, Duteyrat J-L, Augière C, Cortier E, Lapart J-A, Thomas J, Durand B (2016). Transition zone assembly and its contribution to axoneme formation in *Drosophila* male germ cells. J Cell Biol 214, 875–889.

Wilson PG, Zheng Y, Oakley CE, Oakley BR, Borisy GG, Fuller MT (1997). Differential expression of two gamma-tubulin isoforms during gametogenesis and development in *Drosophila*. Dev Biol 184, 207–221.

Zdobnov EM, Tegenfeldt F, Kuznetsov D, Waterhouse RM, Simão FA, Ioannidis P, Seppey M, Loetscher A, Kriventseva EV (2017). OrthoDB v9.1: cataloging evolutionary and functional annotations for animal, fungal, plant, archaeal, bacterial and viral orthologs. Nucleic Acids Res 45, D744–D749.

Zhi E, Li P, Chen H, Xu P, Zhu X, Zhu Z, He Z, Li Z (2016). Decreased expression of KIFC1 in human testes with globozoospermic defects. Genes (Basel) 7, 75.

Zhong L, Belote JM (2007). The testis-specific proteasome subunit Pros 6T of *D. melanogaster* is required for individualization and nuclear maturation during spermatogenesis. Development 134, 3517–3525.